Anapole source based on electric dipole interactions over a low-index dielectric

Muhammad Rizwan Akram[*] and Abbas Semnani[†]

Department of Electrical Engineering and Computer Science, The University of Toledo, Toledo, Ohio, USA

(Received 14 August 2023; revised 24 April 2024; accepted 25 April 2024; published 24 May 2024)

Pursuing nonradiating sources and radiationless motion for accelerated charged particles has captivated physicists for generations. Nonradiating sources represent intricate current-charge configurations that do not emit radiation beyond their source domain. This study investigates a single nonradiating source comprising a low-index dielectric disk excited by a split-ring resonator. Employing analytical and numerical methods, we demonstrate that this configuration supports an anapole state, exhibiting minimal or no radiation, effectively representing a nonradiating source. The radiation suppression is accomplished through the destructive interference of electric dipoles excited on the metallic and dielectric components of the proposed prototype. Transforming the design into a cost-effective device capable of suppressing radiation, we achieve excellent numerical and experimental agreement, affirming the formation of the anapole state using the lowest-order multipoles. Moreover, the devised anapole device is remarkably compact, constructed from a low-index dielectric, and employs readily available components. As a versatile platform, the proposed device can spearhead anapole research for diverse applications, including sensing, wireless charging, radio frequency identification tags, and other nonlinear applications.

DOI: 10.1103/PhysRevApplied.21.054051

I. INTRODUCTION

It is well known that accelerating charges emit electromagnetic (EM) radiation to preserve the stability of matter composed of atoms and molecules. This insight played a crucial role in Bohr's formulation of his postulates and eventually laid the groundwork for quantum mechanics. However, from the early days, scientists have been trying to find confined charge-current configurations that do not radiate. The oscillatory motion of a charged sphere within a single period is one such configuration suggested by Bohm and Weinstein [1], which was later generalized for electron motion in orbits [2]. In this context, a particular charge configuration known as an "anapole" was introduced in elementary particle physics by Zel'dovich [3]. However, the experimental detection of the anapole effect remained challenging until Wood *et al.* successfully observed and measured it in cesium atoms through parity-violating effects [4].

The electrodynamic analogue of an anapole or nonradiating (NR) state can be achieved through the collocation of fundamental electric and magnetic dipoles, along with their toroidal counterparts. This spatial arrangement leads to far-field destructive interference, resulting in minimal radiation due to their similar but out-of-phase field distributions [5]. The toroidal dipole emerges as the third-order term in the Taylor expansion of electromagnetic potentials, complementing other essential dipole moments defined in both Cartesian and spherical harmonics representations [6,7]. A toroidal dipole was experimentally realized in 2010, utilizing the unique response of a metamaterial [8]. In 2013, a microwave anapole was observed experimentally using metasurfaces under plane-wave excitation [9]. Subsequently, in 2015, a simple silicon disk was employed to demonstrate an optical anapole [10].

Due to their exceptional characteristics, including near-field enhancement, high quality factor (Q), and far-field suppression, anapoles have garnered significant attention. This heightened interest has led to a series of advancements in anapole technology [6,11–15], along with the introduction of applications in sensing [16], power transfer [17], and quantum technologies [18]. However, these developments are primarily limited to plane-wave excitation. Expanding the scope of anapole technology to accommodate other excitation methods could unlock additional opportunities for innovative applications beyond the current plane-wave-based structures.

Recently, an anapole source was successfully demonstrated, employing a dipole surrounded by four high-refractive-index cylinders [19]. In this configuration, the central dipole excites an electric toroidal dipole in the surrounding rods, leading to destructive interference and the formation of an anapole state. In another study by Zanganeh *et al.* [20], an anapole state was achieved using a

[*]Corresponding author: muhammadrizwan.akram@utoledo.edu
[†]Corresponding author: abbas.semnani@utoledo.edu

 © 2024 American Physical Society

high-refractive-index cylinder, excited either by an electric dipole with a metallic rod in the middle or by a magnetic dipole with a loop placed inside the cylinder. In the former approach, the superposition of electric dipoles and electric toroidal dipoles forms the anapole state. In contrast, in the latter approach, only magnetic dipoles are superimposed to create an anapole configuration. In a different study, an anapole state was achieved using a high-refractive-index disk excited by an external loop, which led to the superposition of electric dipoles and quadrupoles [17]. However, all these works relied on high-refractive-index materials, which were custom made and not readily available.

As an alternative approach, recent works have revealed the possibility of achieving an anapole state without involving toroidal dipoles. For instance, anapole states have been demonstrated using only electric dipoles and quadrupoles [17]. Numerical studies [20] have explored the superposition of only magnetic dipoles, while theoretical investigations [21] have revealed the possibility of using superimposed electric dipoles alone to achieve an anapole state. However, no experimental demonstrations have been conducted to verify the realization of anapole states solely through basic electric or magnetic dipoles.

This paper introduces and experimentally showcases a microwave anapole source composed of a commercially available and low-index dielectric cylinder with a simple excitation topology. By analyzing the Cartesian multipole expansion in the long-wavelength approximation [7], the feasibility of an anapole formation at the lowest order using only dipole-dipole interactions, as previously explored in theoretical studies [21], is confirmed. For experimental realization, a dielectric cylinder is excited by a microstrip line through a slot on the ground plate. This configuration results in a substantial size reduction compared with existing anapole sources [17,19,20], makes it compatible with printed circuit board (PCB) technology, and enables effective impedance matching, a challenge often encountered in anapole designs.

The proposed design technique is based on the lowest-order electric dipoles, facilitating a compact size even with a low dielectric constant of $\epsilon_r = 12.85$, as opposed to previous works that utilized ϵ_r in the range of 1000 [17,19,20]. The overall size is $0.28\lambda_g$ compared with around 4 λ_g in Refs. [17,19,20], where λ_g represents the wavelength in the dielectric medium, equating to an almost 14 times reduction in size. Moreover, its compatibility with existing fabrication technologies allows for commercial prototyping and facilitates the rapid development of various anapole-based applications in wireless sensing, charging, and nonlinear electromagnetics and optics.

II. THEORY AND DESIGN

As depicted in Fig. 1, the proposed anapole design consists of two metallic rods connected by a metallic strip to form a loop. This loop radiates like an electric dipole and induces a nearly equal but opposite electric dipole in the dielectric cylinder. Thus, the two dipoles destructively interfere, resulting in an anapole state. The design's nonradiating response is sensitive to the gap between the two metallic rods; a narrower gap leads to lower radiation, consistent with theoretical investigations [21].

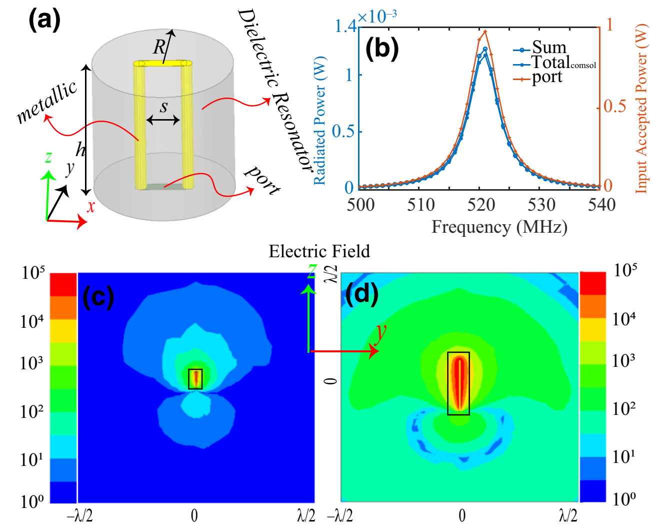

FIG. 1. (a) Schematic of the proposed anapole design with a dielectric cylinder of radius $R = 6$ mm and height $h = 40$ mm, with metallic vias each of radius $r = 0.5$ mm and a center-to-center distance of $s = 0.6$ mm, forming a split-ring resonator (SRR). The dielectric cylinder is made of Rogers TMM13i laminate with permittivity of 12.85 and $\tan\delta = 1.9 \times 10^{-3}$. (b) The radiated power is evaluated through numerical Cartesian multipole expansion, and the total power accepted by the device is in red. The simulated near electric field for (c) the proposed nonradiating (anapole) source and (d) the loop without the dielectric cylinder, which acts as a radiating source.

The radiation performance of the introduced anapole design is initially explored through numerical simulations using COMSOL Multiphysics. As depicted in Fig. 1(b), at a sample design's resonant frequency of 520 MHz, the maximum radiation is just 1.4 mW out of the total input power of 1 W, representing only 0.14% radiation. Remarkably, only 0.04% of this radiation is attributed to the electric dipoles, and the rest is from the magnetic dipole component, as plotted in detail in Fig. 1(b).

The metallic loop without the dielectric cylinder is also simulated for comparison. Resonance is observed at 1.812 GHz with a radiation efficiency exceeding 98%. The near-field plots of the y-z plane for both nonradiating and radiating cases are illustrated in Figs. 1(c) and 1(d), respectively. The remarkable confinement of electric and magnetic fields in the device's proximity, coupled with the significant suppression of far-field radiation, provides compelling evidence of the successful formation of an anapole state. The reduction rate is over 100 times

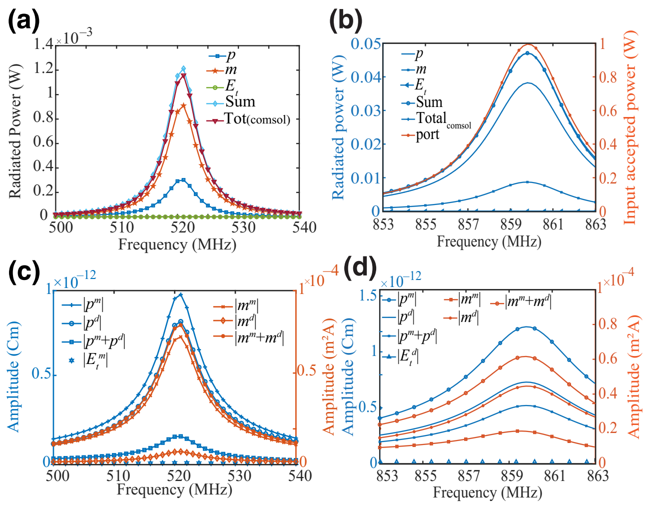

FIG. 2. Extracted radiated powers computed using Cartesian multipole expansion and numerical methods (a) for the loop embedded dielectric cylinder depicted in Fig. 1 with $s = 0.6$ mm and with input impedance of around 150 kΩ and (b) for the practical anapole device shown in Fig. 3. Similarly, electric and magnetic dipoles are separately evaluated for the metallic and the dielectric parts for (c) the conceptual design of Fig. 1 and (d) the practical anapole device of Fig. 3, where p represents electric, m magnetic, subscript t toroidal, superscript m metal, and d dielectric.

in the nonradiating state compared with the radiating state.

A Cartesian multipole expansion of the EM fields is conducted to gain a profound understanding of the underlying nonradiating mechanism. The results of radiation suppression can be observed in Fig. 2(a). As radiation contributions are solely attributed to electric and magnetic dipoles, separate characterizations of these dipoles on both metallic loop and dielectric sections are performed, with the results illustrated in Figs. 2(c). These results reveal that the electric dipoles induce a destructive interference on the loop, similar to that observed in the dielectric region, whereas the magnetic fields exhibit constructive interference. Additionally, the toroidal dipoles contribute almost negligibly to the overall response. Consequently, the expression for this nonradiating electric source can be represented as [22]:

$$P \sim |p^m + p^d|^2 = |p^m|^2 + |p^d|^2 + 2RE[p^m p^d *]. \quad (1)$$

Here, p^m is the electric response of the metallic loop, p^d represents the electric response of the dielectric cylinder, and $(p^m + p^d)$ is the total electric response of the structure.

For experimental verification, a cylindrical disk is crafted from a Rogers TMM13i laminate, featuring a thickness of 3.81 mm and 35-μm copper cladding. For the feeding, another layer is fashioned from a 1.27-mm-thick Rogers TMM6 laminate with the same 35-μm cladding.

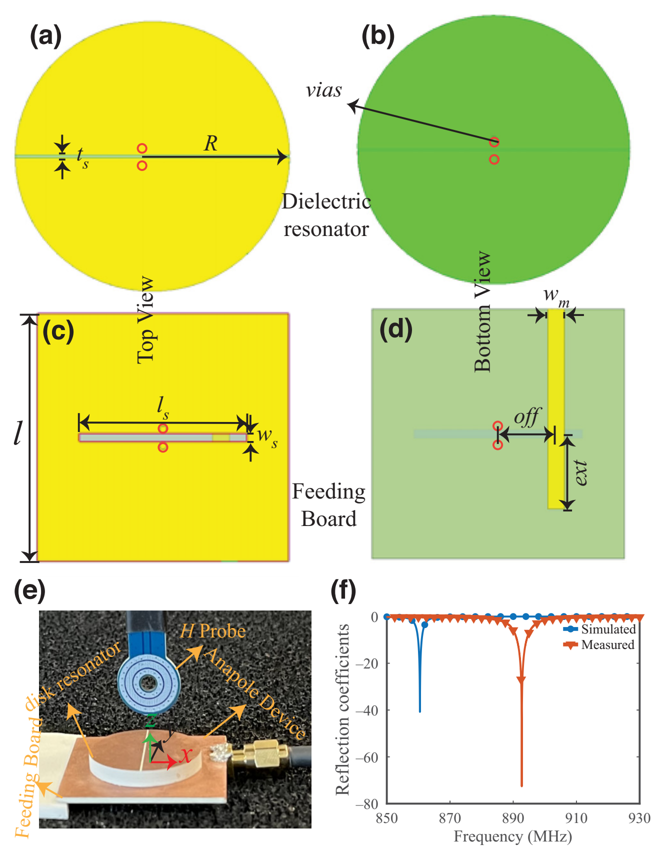

FIG. 3. Top (a),(c) and bottom (b),(d) views of the dielectric resonator and the feeding board of the anapole device with $R = 14$ mm, thickness of the dielectric cylinder $h = 3.81$ mm, thickness of feed board $h_2 = 1.27$ mm, $l_s = 20$ mm, $l = 40$ mm, $w_m = 2$ mm, ext = 9 mm, off = 6.9 mm, $w_s = 1$ mm, $t_s = 0.3$ mm, and $s = 1.2$ mm. The cylindrical resonator is made of TMM13i with permittivity of $\epsilon_r = 13$ and $\tan\delta = 1.9 \times 10^{-3}$. The bottom board is made of TMM6 with permittivity of $\epsilon_r = 6$ and $\tan\delta = 2.3 \times 10^{-3}$. (e) The fabricated anapole device is connected to the transmitter port of a vector network analyzer (VNA), with an H-field probe attached to the receiver port of the VNA, configured for H_y measurements. The bottom board is the feeding part coupled to the disk using a slot coupling topology. (f) The simulated and measured reflection coefficients showcase a solid resonance.

The assembly process involves aligning the disk with the feeding board using vias and holes, which are then secured using silver epoxy. The detailed design is shown in Figs. 3(a)–3(e). The microwave signal is fed through a 50-Ω microstrip line coupled to the dielectric resonator through a slot etched on the ground plane of the TMM6 feeding board. A top metallic pattern is utilized atop the dielectric resonator for further size reduction. The resulting prototype is remarkably compact, with its largest dimension lower than 0.1λ. A monopole and a loop receiver acting as E and H probes are utilized for field measurements.

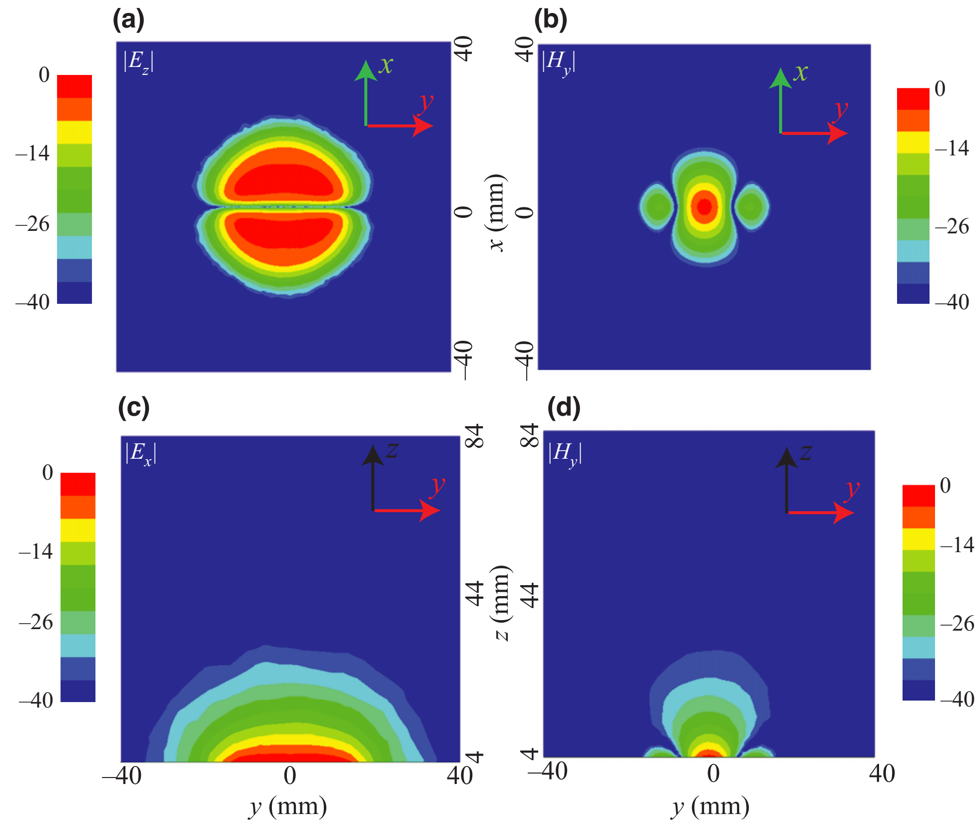

FIG. 4. The simulated (a) E_z for the x-y plane at a height of $z = 4$ mm, (b) H_y for the x-y plane at a height of $z = 4$ mm, (c) E_x for the y-z plane with $x = 0$, and (d) H_y for the y-z plane with $x = 0$. The color bars correspond to a dB scale.

III. RESULTS AND DISCUSSION

The simulated and measured reflection coefficients are plotted in Fig. 3(f). A strong resonance is measured at 893 MHz, 30 MHz off compared with the simulation. This variance is attributed to the manual alignment of the disk and the fabrication tolerances. Subsequently, a Cartesian multipole expansion analysis is conducted, showing that less than 50 mW out of 1 W accepted power is radiated, with a contribution of only 35 mW from the electric dipoles, as seen in Figs. 2(b) and 2(d). Further reduction of this radiation is feasible by narrowing the gap between the vias; however, practical limitations about fabrication tolerances should be considered. Moreover, the individual contributions of electric and magnetic dipoles are evaluated separately on the metallic and dielectric portions of the structure. Although the proof of concept is performed for the microwave regime, it could potentially be extendable to terahertz and/or optical regimes depending upon the availability of specialized coating [23]. Moreover, loss compensation using gain media [24] would be an interesting avenue to push the complete loss-free anapole design to facilitate lasing action.

The near-field investigation of the prototype is conducted through numerical simulations and experimental measurements, as depicted in Figs. 4 and 5. Among the field components, only E_x, E_z, and H_y demonstrate significant contributions. For conciseness, we focus on measuring and comparing only the E_z and H_y components with the simulation results.

A monopole and a loop-shaped probe are employed for E-field and H-field measurements, respectively. As shown in Fig. 3(c), the probes are oriented to align their axes along the y axis to optimally couple with the maximum H_y field and vertically for the monopole probe to couple maximally with E_z. The field plots exhibit an excellent agreement between the simulations and measurements, revealing a robust suppression of the fields, confined within a few fractions of a wavelength away from the device. Moreover, the decay of the electric field at the resonance frequency and two adjacent frequencies is compared with distance from the device alongside $1/R^2$. As depicted in Fig. 6, the electric field decay is significantly higher at the anapole frequency than at the other frequencies, which exhibit a decay rate more closely aligned with $1/R^2$. This striking observation serves as a clear indication of the successful formation of the anapole state.

An anapole state does not inherently arise as a natural eigenstate within an open cavity, as highlighted in previous literature [25]. It only manifests in the presence

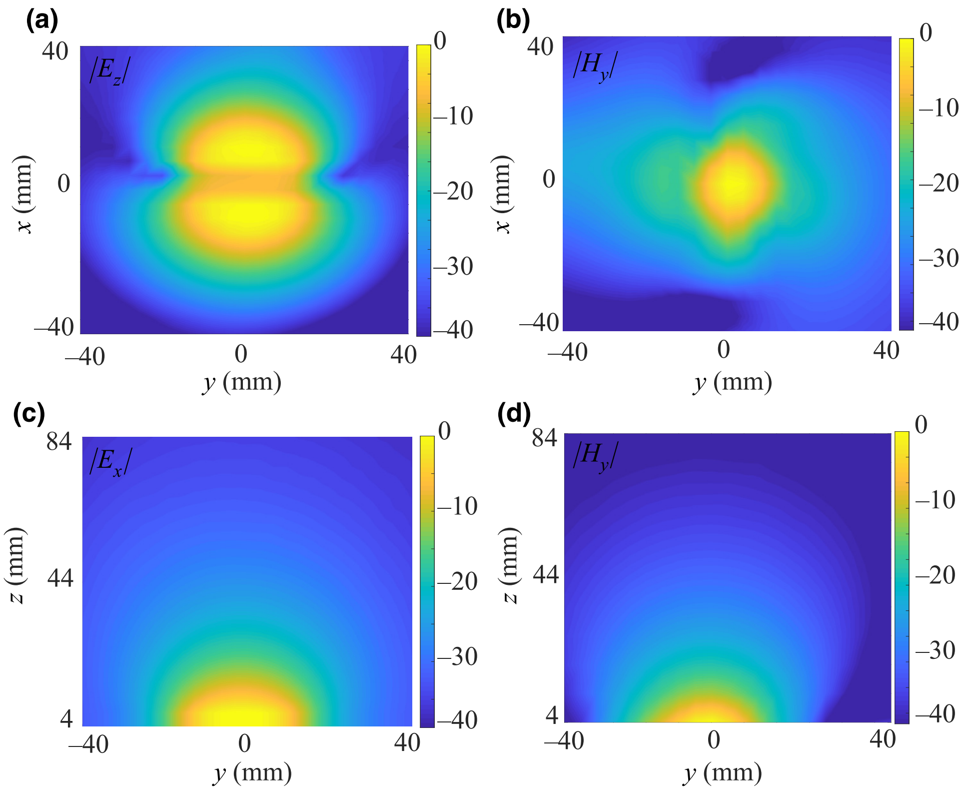

FIG. 5. The measured (a) E_z for the x-y plane at a height of $h = 4$ mm, (b) h_Y for the x-y plane at a height of $h = 4$ mm, (c) E_x for the y-z plane with $x = 0$, and (d) H_y for the y-z plane with $x = 0$. The color bars correspond to a dB scale.

of an incident field, setting it apart from bound states in a continuum or traditional eigenstates [26–31]. However, the anapoles are externally excited and sustained, distinct from scattering effects. The fact that the anapole state results in the cancellation of far-field interaction of various dipolar responses enables a near-field enhancement around the device, which can be utilized for many applications. Furthermore, the cloaked devices depicted in Refs. [32–36], which similarly exhibit no external scattering, stand distinct from anapoles due to the underlying realization mechanism. Unlike anapoles, these devices are crafted from multilayered particles, wherein the cumulative dipolar response on each layer nullifies, resulting in a nonscattering cross section.

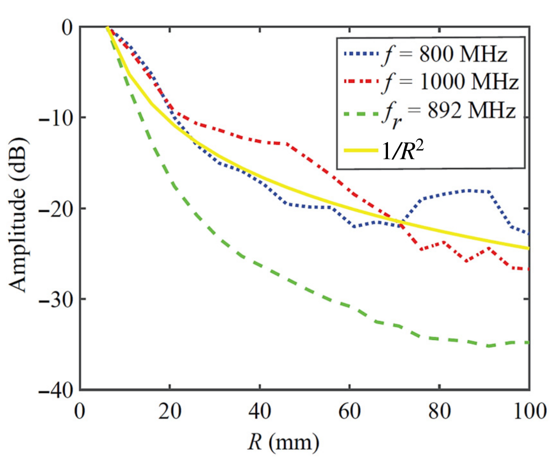

FIG. 6. Measured electric field amplitude on the vertical axis plotted against the distance (R) between transmitter and receiver on the horizontal axis, where f_r represents the anapole frequency.

IV. CONCLUSION

A technique to achieve the lowest-order anapole source is introduced, relying solely on electric dipole interactions. In this technique, effective radiation suppression can be achieved by leveraging electric dipole interactions. To realize experimentally, a low-index dielectric is employed in a hybrid structure comprising a dielectric disk inserted with a metallic loop. The design is successfully evaluated, both numerically and experimentally, confirming its capability of achieving the desired radiation suppression. The proposed technique also boasts compactness and utilizes a low-index dielectric, which holds promise for various anapole applications. These applications encompass various fields, including sensing, wireless power transfer, and nonlinear interactions.

ACKNOWLEDGMENTS

This work was supported by the National Science Foundation (NSF) under Grant No. ECCS-2102100.

APPENDIX A: CARTESIAN MULTIPOLE EXPANSION

Cartesian multipole expansion is employed to evaluate the strength of electric and magnetic dipoles, quadrupole, and toroidal dipole and their contribution to the far-field radiation over the proposed anapole device, as shown in Fig. 2. This is done by integrating the current density within the dielectric volume and on the metallic parts through the postprocessing options available in COMSOL Multiphysics. The involved Cartesian multipoles are defined as

$$p_i = \frac{1}{iw}\int J_i dv, \tag{A1}$$

$$m_j = \frac{1}{2}\int (r\times J)_j dv, \tag{A2}$$

$$Q^e_{ij} = \frac{1}{iw}\int \left(r_j J_i + r_i J_j + \frac{2}{3}\delta_{ij}(r\cdot j)\right)dv, \tag{A3}$$

$$Q^m_{ij} = \frac{1}{3}\int ((r\times J)_i r_j + (r\times J)_j r_i)dv, \tag{A4}$$

$$T^e_i = \frac{1}{10}\int ((r\cdot J)r_i - 2r^2 J_i)dv. \tag{A5}$$

Here, subscripts $i, j = x, y, z$, superscripts e and m represent electric and magnetic, respectively, and symbols p, m, Q, and T represent electric dipole, magnetic dipole, quadrupole, and toroidal dipole, respectively. J is the total of surface current and induced currents inside the device:

$$J = iw\epsilon_0(\epsilon_r - 1)E, \tag{A6}$$

where ϵ is the angular frequency, ϵ_0 is the vacuum permittivity, ϵ_r is the complex relative permittivity of the dielectric, and E is the electric field. The total radiation intensity of these multipoles can then be calculated using

$$I_{\text{Total}} = \frac{k^4}{12\pi\epsilon_0^2 c\mu_0}\left|p - \frac{ik}{c}T^e\right|^2 + \frac{k^4}{12\pi\epsilon_0 c}|m|^2 + \frac{k^6}{160\pi\epsilon_0^2 c\mu_0}|Q^e_{ij}|^2 + \frac{k^6}{160\pi\epsilon_0 c}|Q^m_{ij}|^2. \tag{A7}$$

APPENDIX B: RADIATING LOOP ANTENNA

The loop inside the dielectric is used as a radiating antenna, which is then excited with a lumped port using high-frequency simulation software. The resonance is obtained around 1.812 GHz, for which impedance is matched using port impedance to 280 kΩ. More than 95% input energy is coupled with the device, as shown in Fig. 7. The electric field of the loop antenna is plotted in Fig. 1(d) for a direct comparison of the nonradiating mode.

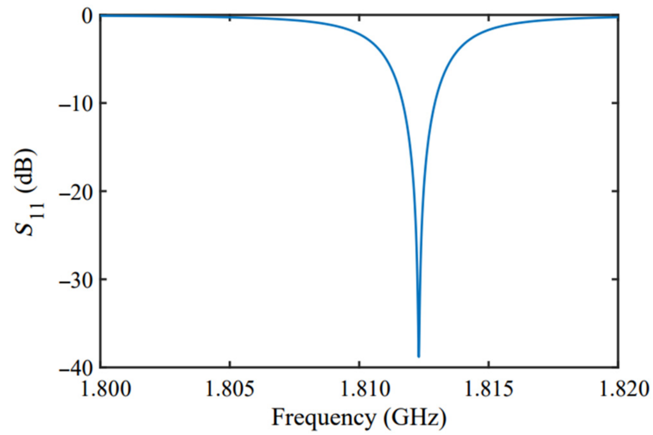

FIG. 7. Reflection coefficient for the loop antenna.

APPENDIX C: EXPERIMENTAL EVALUATION

The experimental studies of the electric and magnetic field characteristics of the NR electric source prototype are performed at the resonance frequency of 892 MHz. Figure 8 shows the automated measurement setup, which can scan electric fields in a three-dimensional domain from 500 × 500 × 300 mm^3. The prototype monopole and loop-type electromagnetic compatibility near-field probes are used to evaluate the electric and magnetic fields. The numerical investigations reveal that only E_x, E_z, and H_y field distributions are significant around the NR electric source. The device is connected to port 1 of the VNA, and the probe is connected to port 2. For H_y measurements, the loop probe is oriented in such a way that the axis of the loop is aligned to the y axis of the device to ensure maximum coupling. In this way, S_{21} measures the H_y component, and similarly, for E_z measurements, the monopole

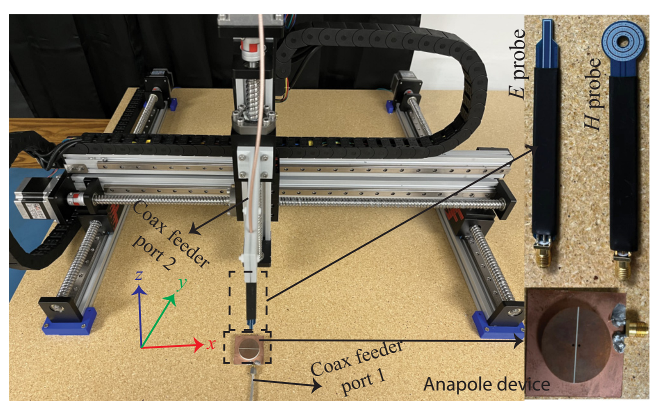

FIG. 8. Experimental setup along with E and H probes and anapole device.

probe is aligned in the z direction of the device to ensure maximum coupling. The measurements are performed in two planes: the x-y plane of 80×80 mm^2 with a probe-to-device distance of nearly 4 mm and the y-z plane of 80×88 mm^2 for H_y and 80×48 mm^2 with a resolution of 1 mm. The measured results are shown in Fig. 6, which are in good agreement with the numerical results in Fig. 5, indicating the radiationless performance of the prototype.

[1] D. Bohm and M. Weinstein, The self-oscillations of a charged particle, Phys. Rev. **74**, 1789 (1948).

[2] G. H. Goedecke, Classically radiationless motions and possible implications for quantum theory, Phys. Rev. **135**, B281 (1964).

[3] I. B. Zel'Dovich, Electromagnetic interaction with parity violation, Sov. Phys. JETP **6**, 1184 (1958).

[4] C. Wood, S. Bennett, D. Cho, B. Masterson, J. Roberts, C. Tanner, and C. E. Wieman, Measurement of parity nonconservation and an anapole moment in cesium, Science **275**, 1759 (1997).

[5] Y. Yang and S. I. Bozhevolnyi, Nonradiating anapole states in nanophotonics: From fundamentals to applications, Nanotechnology **30**, 204001 (2019).

[6] E. A. Gurvitz, K. S. Ladutenko, P. A. Dergachev, A. B. Evlyukhin, A. E. Miroshnichenko, and A. S. Shalin, The high-order toroidal moments and anapole states in all-dielectric photonics, Laser & Photonics Rev. **13**, 1800266 (2019).

[7] R. Alaee, C. Rockstuhl, and I. Fernandez-Corbaton, An electromagnetic multipole expansion beyond the long-wavelength approximation, Opt. Commun. **407**, 17 (2018).

[8] T. Kaelberer, V. Fedotov, N. Papasimakis, D. Tsai, and N. Zheludev, Toroidal dipolar response in a metamaterial, Science **330**, 1510 (2010).

[9] V. A. Fedotov, A. Rogacheva, V. Savinov, D. P. Tsai, and N. I. Zheludev, Resonant transparency and non-trivial nonradiating excitations in toroidal metamaterials, Sci. Rep. **3**, 2967 (2013).

[10] A. E. Miroshnichenko, A. B. Evlyukhin, Y. F. Yu, R. M. Bakker, A. Chipouline, A. I. Kuznetsov, B. Luk'yanchuk, B. N. Chichkov, and Y. S. Kivshar, Nonradiating anapole modes in dielectric nanoparticles, Nat. Commun. **6**, 8069 (2015).

[11] P. Kapitanova, E. Zanganeh, N. Pavlov, M. Song, P. Belov, A. Evlyukhin, and A. Miroshnichenko, Seeing the unseen: Experimental observation of magnetic anapole state inside a high-index dielectric particle, Ann. Phys. **532**, 2000293 (2020).

[12] B. Luk'yanchuk, R. Paniagua-Domínguez, A. I. Kuznetsov, A. E. Miroshnichenko, and Y. S. Kivshar, Hybrid anapole modes of high-index dielectric nanoparticles, Phys. Rev. A **95**, 063820 (2017).

[13] B. Luk'yanchuk, R. Paniagua-Domínguez, A. I. Kuznetsov, A. E. Miroshnichenko, and Y. S. Kivshar, Suppression of scattering for small dielectric particles: Anapole mode and invisibility, Philos. Tran. R. Soc.: Math. Phys. Eng. Sci. **375**, 20160069 (2017).

[14] J. A. Parker, H. Sugimoto, B. Coe, D. Eggena, M. Fujii, N. F. Scherer, S. K. Gray, and U. Manna, Excitation of nonradiating anapoles in dielectric nanospheres, Phys. Rev. Lett. **124**, 097402 (2020).

[15] V. A. Zenin, A. B. Evlyukhin, S. M. Novikov, Y. Yang, R. Malureanu, A. V. Lavrinenko, B. N. Chichkov, and S. I. Bozhevolnyi, Direct amplitude-phase near-field observation of higher-order anapole states, Nano Lett. **17**, 7152 (2017).

[16] C. Zhang, T. Xue, J. Zhang, Z. Li, L. Liu, J. Xie, J. Yao, G. Wang, X. Ye, and W. Zhu, Terahertz meta-biosensor based on high-Q electrical resonance enhanced by the interference of toroidal dipole, Biosensors Bioelectron. **214**, 114493 (2022).

[17] E. Zanganeh, M. Song, A. C. Valero, A. S. Shalin, E. Nenasheva, A. Miroshnichenko, A. Evlyukhin, and P. Kapitanova, Nonradiating sources for efficient wireless power transfer, Nanophotonics **10**, 4399*** (2021).

[18] V. Savinov, N. Papasimakis, D. Tsai, and N. Zheludev, Optical anapoles, Commun. Phys. **2**, 69 (2019).

[19] N. A. Nemkov, I. V. Stenishchev, and A. A. Basharin, Nontrivial nonradiating all-dielectric anapole, Sci. Rep. **7**, 1064 (2017).

[20] E. Zanganeh, A. Evlyukhin, A. Miroshnichenko, M. Song, E. Nenasheva, and P. Kapitanova, Anapole meta-atoms: Nonradiating electric and magnetic sources, Phys. Rev. Lett. **127**, 096804 (2021).

[21] J. R. Zurita-Sánchez, Anapole arising from a Mie scatterer with dipole excitation, Phys. Rev. Res. **1**, 033064 (2019).

[22] A. B. Evlyukhin, T. Fischer, C. Reinhardt, and B. N. Chichkov, Optical theorem and multipole scattering of light by arbitrarily shaped nanoparticles, Phys. Rev. B **94**, 205434 (2016).

[23] See https://www.altechna.com/products/metallic-coated-optics/metallic-coated-optics/.

[24] E. I. Kirby, J. M. Hamm, T. W. Pickering, K. L. Tsakmakidis, and O. Hess, Evanescent gain for slow and stopped light in negative refractive index heterostructures, Phys. Rev. B **84**, 041103 (2011).

[25] F. Monticone, D. Sounas, A. Krasnok, and A. Alù, Can a nonradiating mode be externally excited? Nonscattering states versus embedded eigenstates, ACS Photonics **6**, 3108 (2019).

[26] C. W. Hsu, B. Zhen, A. D. Stone, J. D. Joannopoulos, and M. Soljačić, Bound states in the continuum, Nat. Rev. Mater. **1**, 1 (2016).

[27] F. Monticone and A. Alu, Embedded photonic eigenvalues in 3D nanostructures, Phys. Rev. Lett. **112**, 213903 (2014).

[28] C. W. Hsu, B. Zhen, J. Lee, S.-L. Chua, S. G. Johnson, J. D. Joannopoulos, and M. Soljačić, Observation of trapped light within the radiation continuum, Nature **499**, 188 (2013).

[29] M. G. Silveirinha, Trapping light in open plasmonic nanostructures, Phys. Rev. A **89**, 023813 (2014).

[30] F. Monticone, H. M. Doeleman, W. Den Hollander, A. F. Koenderink, and A. Alù, Trapping light in plain sight: Embedded photonic eigenstates in zero-index metamaterials, Laser & Photonics Rev. **12**, 1700220 (2018).

[31] H. M. Doeleman, F. Monticone, W. den Hollander, A. Alù, and A. F. Koenderink, Experimental observation of a polarization vortex at an optical bound state in the continuum, Nat. Photonics **12**, 397 (2018).

[32] A. Alù and N. Engheta, Achieving transparency with plasmonic and metamaterial coatings, Phys. Rev. E **72**, 016623 (2005).

[33] A. Alù and N. Engheta, Multifrequency optical invisibility cloak with layered plasmonic shells, Phys. Rev. Lett. **100**, 113901 (2008).

[34] B. Edwards, A. Alù, M. G. Silveirinha, and N. Engheta, Experimental verification of plasmonic cloaking at microwave frequencies with metamaterials, Phys. Rev. Lett. **103**, 153901 (2009).

[35] A. Alù and N. Engheta, Cloaked near-field scanning optical microscope tip for noninvasive near-field imaging, Phys. Rev. Lett. **105**, 263906 (2010).

[36] F. Bilotti, S. Tricarico, F. Pierini, and L. Vegni, Cloaking apertureless near-field scanning optical microscopy tips, Opt. Lett. **36**, 211 (2011).